

ICON: an adaptation of infinite HMMs for time traces with drift

I Sgouralis and S Pressé

Abstract

Bayesian nonparametric methods have recently transformed emerging areas within data science. One such promising method, the infinite hidden Markov model (iHMM), generalizes the HMM which itself has become a workhorse in single molecule data analysis. The iHMM goes beyond the HMM by self-consistently learning all parameters learned by the HMM in addition to learning the number of states without recourse to any model selection steps. Despite its generality, simple features (such as drift), common to single molecule time traces, result in an over-interpretation of drift and the introduction of artifact states. Here we present an adaptation of the iHMM that can treat data with drift originating from one or many traces (e.g. FRET). Our fully Bayesian method couples the iHMM to a continuous control process (drift) self-consistently learned while learning all other quantities determined by the iHMM (including state numbers). A key advantage of this method is that all traces – regardless of drift or states visited across traces – may now be treated on an equal footing thereby eliminating user-dependent trace selection (based on drift levels), pre-processing to remove drift and post-processing model selection on state number.

1 Introduction

Single molecule experiments – such as single molecule FRET (smFRET) [1] or force spectroscopy [2] – exhibit discrete transitions between states or molecular conformations. These transitions are often idealized as memoryless (Markovian) processes and, as a result, hidden Markov models (HMM) [3] – describing Markov transitions obscured by noise – naturally arise in single molecule data analysis [4, 5, 6, 7, 8, 9]. While traditional HMMs are used to find kinetics of transition between states, they cannot learn the number of states. Indeed, for the HMM to apply in the first place, the number of states that the system may visit over the course of a time trace must be fixed *a priori* [5].

Following a HMM analysis, model selection criteria are often invoked to discriminate between various models – labeled “parametric” because they entail a *finite* set of parameters – with a different number of states [9, 10, 4]. This approach breaks down the full optimization problem of i) enumerating the states and ii) parametrizing the model into two disjoint operations that may not result in an optimal global solution.

It is for this reason that a nonparametric [11] realization of the HMM, the so called *infinite hidden Markov model* (iHMM) was developed [12]. Since its introduction, the iHMM has provided a principled method to perform time series analysis in machine learning applications. Despite the success of iHMMs outside Biology, to our knowledge only a single proof-of-concept paper illustrating the potential of iHMMs to single molecule Biophysics has appeared [13].

By contrast to HMMs having a fixed number of states, the nonparametric adaptation of the HMM, the iHMM, may recruit from an infinite pool new states on the basis of the available data [12, 14, 11] without ever prespecifying a total number as would be the case with the HMM.

While promising, the iHMM’s flexibility – lending the iHMM its intrinsic ability to learn the number of conformational states, say, visited by a single molecule – can become an important weakness. As an example, iHMMs would deal with drift, encountered throughout single molecule experiments, by adding “artifact states”. To date, just as it is common to prespecify the number of states in an HMM, it is also common practice to de-drift

(or de-trend) the time traces using standard time series methods, e.g. [15, 16, 17], and subsequently analyze the data with an HMM [18]. In principle, the same may be done with iHMMs. The catch however is that, at best, de-drifting separately from the rest of the data analysis leads to a subsequent estimation of the states conditioned on the de-drifting procedure which, in turn, may again lead to suboptimal estimates for the states as conceptually illustrated in Fig. 1.

In fact, it is specifically to avoid such suboptimal estimates (in this case to estimate noise properties while estimating transition probabilities) that HMMs exist in the first place: they learn transition probabilities while de-noising a time trace self-consistently.

Here we take the same logic some steps further and adapt the iHMM to make it useful for applications in Biophysics where traces are often corrupted by drift. In particular, we provide a novel formulation of iHMMs with a fully Bayesian consideration of drift. We adapt the iHMM to: i) incorporate information from multiple traces (e.g. recordings from different channels) – typically available in many setups such as FRET measurements – and; ii) infer the drift simultaneously, and thus self-consistently, while learning the number of states along with their transition kinetics and emission properties.

The remainder of this paper is organized as follows. In Methods, we present the formulation of the iHMM and its extensions leading to ICON (Infinite HMM coupled to a continuous CONtrol process, i.e. the drift) which are required for the subsequent analysis. In the Results, we present selected applications of the proposed method using both synthetic and experimental datasets. Lastly, in the Discussion, we discuss the broader potential of the method to Biophysics. Additional remarks and an implementation of the proposed method can be found in the supporting materials.

2 Methods

Here we first describe the basic formulation of the HMM as it applies to biophysical data allowing us to introduce the iHMM as its generalization. Subsequently, we introduce ICON as an extension of the iHMM. While the literature on iHMMs is currently intended for specialized audiences in Statistics, and the mathematics themselves are quite technical [14], we provide a more detailed presentation of the iHMM dedicated to physical scientists in a companion article [19].

We begin by assuming that a molecule under investigation switches, on or slower than the data acquisition timescale, discretely between different conformational states that we denote σ_k , where $k = 1, 2, \dots$ labels these conformations, Fig 2. While we will keep referring to single molecules for simplicity, it is understood that time traces similar to the ones we consider may also be generated from experiments on molecular complexes involving many biomolecules [20].

Each conformation σ_k yields or “emits” observations x according to a unique probability distribution $F_{\sigma_k}(x)$. To model each of these distributions, we assume a generic form that depends on some state specific parameters ϕ_{σ_k} . In this study, for simplicity, we assume Gaussian emissions

$$F_{\sigma_k}(x) = \sqrt{\frac{\tau_{\sigma_k}}{2\pi}} \exp\left(-\frac{\tau_{\sigma_k}}{2}(x - \mu_{\sigma_k})^2\right) \quad (1)$$

where, for this specific example, the parameters include the Gaussian mean and precision, $\phi_{\sigma_k} = (\mu_{\sigma_k}, \tau_{\sigma_k})$. In general, the method is readily customized to treat any family of emission distribution, such as Poisson, that may

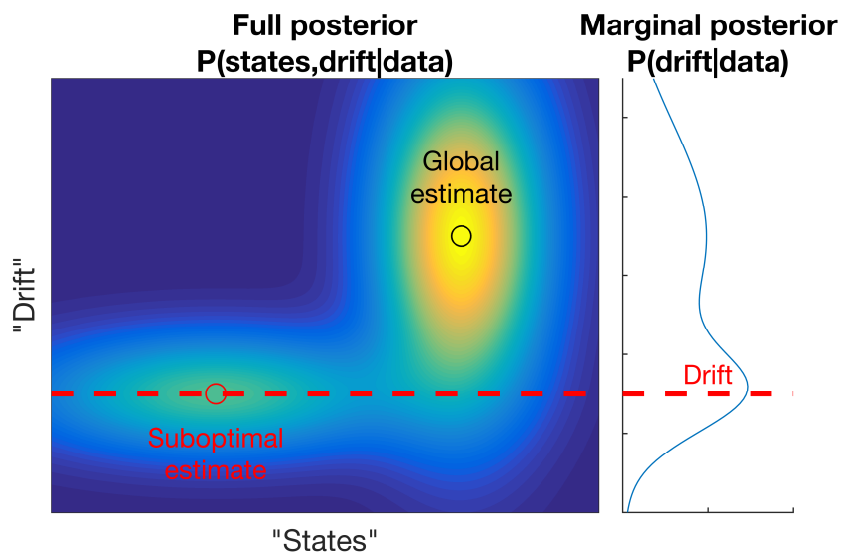


Figure 1: **A conceptual illustration of the pitfalls of independent de-drifting in the analysis of single molecule measurements.** Here, the axes represent abstractions of a single molecule's states and drift. The model's posterior probability distribution (main panel) is color coded with brighter colors corresponding to higher probability. Inference primarily seeks to identify the most likely states estimate, i.e. the estimate with the highest posterior probability. In cases where the posterior has multiple maxima as shown, processing for drift independently of the states might lead to inaccurate estimation of drift (dashed line). Here, drift estimation is based on the posterior distribution marginalized over the states (left panel). Subsequently, processing of the states, which in this case will be restricted only along the dashed line, will result in less likely state number estimates. By contrast, simultaneous processing of the states and drift as we proposed herewith allow inference in the full plane. Hence the global maximum, i.e. the most likely combination of states and drift, can be readily identified. For an explicit example utilizing inaccurate drift estimates see lower panel of Fig. 5 below. Ignoring drift in this example is equivalent to misidentifying a flat drift profile and sub-optimality of the inferred states is demonstrated by the identification of artifact states.

more accurately capture experimental conditions [21].

During the experiment, emissions are collected at equidistant time intervals or “steps” t_n , where $n = 1$ and N denote the first and last measurements. At each time step, we denote the corresponding emission as x_n and the underlying conformation as s_n . That is, during the experiment, the biomolecule chooses s_n from the set $\{\sigma_1, \sigma_2, \dots\}$ and emits x_n according to $F_{s_n}(x_n)$; for an illustration see Fig. 2.

To model the sequence of the successive conformations $s_1 \rightarrow s_2 \rightarrow \dots \rightarrow s_N$ that the biomolecule attains during the experiment time course, HMMs assume Markovian dynamics [3, 9] leading to the following scheme

$$s_n | s_{n-1} \sim \text{Cat}(\tilde{\pi}_{s_{n-1}}), \quad (2)$$

$$x_n | s_n \sim F_{s_n}. \quad (3)$$

Here, $\tilde{\pi}_{s_{n-1}} = (\pi_{s_{n-1} \rightarrow \sigma_1}, \pi_{s_{n-1} \rightarrow \sigma_2}, \dots)$ gathers the probabilities of switching from s_{n-1} to any σ_k , and $\text{Cat}(\tilde{\pi}_{s_{n-1}})$ denotes the categorical probability distribution. In other words, $\pi_{s_{n-1} \rightarrow \sigma_k}$ is the probability of jumping from s_{n-1} to σ_k .

From the HMM model, Eqns. (2)–(3), the logic proceeds forward as follows: we derive a likelihood (or a posterior probability) of observing the time trace from the model and subsequently maximize this likelihood (or posterior probability) to find the values of the model parameters [3]. These parameters include the transition probabilities $\pi_{\sigma_k \rightarrow \sigma_j}$ between all pairs of states (σ_k and σ_j) and all emission parameters ϕ_{σ_k} .

The iHMM is more complex than the HMM and relies on mathematics outside the scope of this paper that we have however detailed in a companion article [19].

In the iHMM, the precise number of conformational states attainable by a biomolecule – and thus the size of $\{\sigma_1, \sigma_2, \dots\}$ – is *a priori* left unspecified [12]. Starting from a conformation s_n at time step n , the biomolecule is allowed to choose between a potentially infinite number of conformations σ_k for the next time step. Only the form of the prior on those transition probabilities – in other words, a probability distribution over $\tilde{\pi}_{\sigma_k}$ – determines whether the system visits a new or an already visited state at each time step. As explained in Ref. [14] and Ref. [19], this prior is a *hierarchical Dirichlet process* which, in one of its realizations, takes the form

$$\tilde{\beta} \sim \text{GEM}(\gamma), \quad (4)$$

$$\tilde{\pi}_{\sigma_k} | \tilde{\beta} \sim \text{DP}(\alpha, \tilde{\beta}), \quad (5)$$

$$\phi_{\sigma_k} \sim H, \quad (6)$$

where $\text{GEM}(\gamma)$ and $\text{DP}(\alpha, \tilde{\beta})$ denote a stick-breaking and a Dirichlet process with concentration parameters γ and α , respectively, and $\tilde{\beta} = (\beta_{\sigma_1}, \beta_{\sigma_2}, \dots)$ is the base distribution [14]. Here, H denotes the prior probability distribution of the emission parameters ϕ_{σ_k} . Throughout this study, for H , we adopt the conditionally-conjugate model developed in Ref. [23], which allows simultaneous learning of μ_{σ_k} and τ_{σ_k} ; see Eq. (1). The full set of equations formulating iHMM is listed in the supporting materials.

The iHMM captures the fact that measurements are contaminated with noise described by the state-dependent emission distributions $F_{\sigma_k}(x)$. However, perhaps even more importantly, time traces may also be contaminated with drift [1] which the model – as written in Eqns. (2)–(6) – does not capture. This happens because iHMMs model abrupt transitions in traces which, for the moment, excludes the possibility of a slowly-evolving drift that requires a *continuous* process instead.

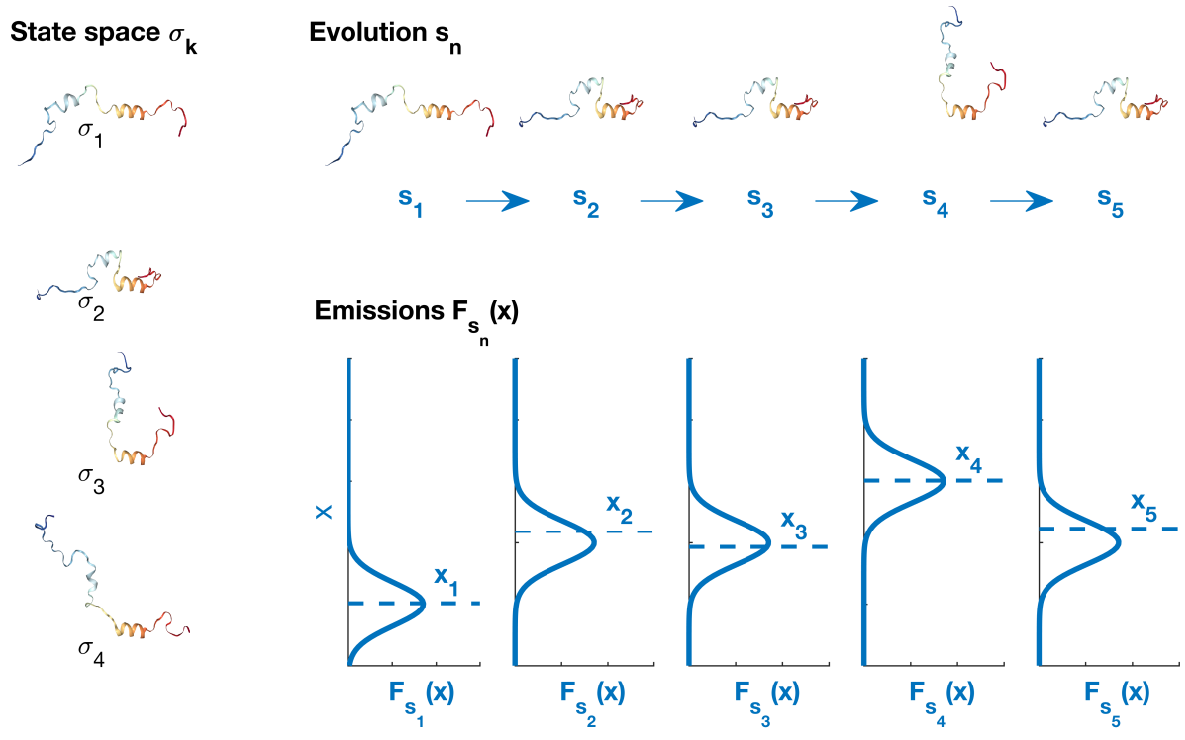


Figure 2: **Illustration of a hypothetical biomolecule with four or potentially more conformational states.** *Left:* the biomolecule's conformations σ_k . *Upper right:* Sequence of conformational changes at each time step, s_n . For sake of illustration here, only conformations σ_1 , σ_2 , and σ_3 are visited, while σ_4 remains unvisited throughout the time trace. *Lower right:* Corresponding emission distributions $F_{s_n}(x_n)$ of the visited states – since the system remains in the same state at time steps 2 and 3, those emission distributions are identical. Dashed lines represent the emissions x_n at corresponding times t_n . For the biomolecule's illustration, we used data from Ref. [22].

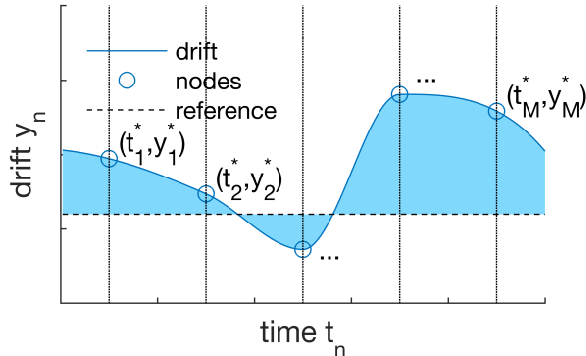


Figure 3: **Drift representation for a single experimental trace.** Circles mark the interpolation nodes (t_m^*, y_m^*) , the solid line marks the drift contribution to the time trace $\bar{y} = (y_1, y_2, \dots, y_N)$ and the dashed line marks the reference level y_{ref}^* which is set to the zero emission level. The shaded region represents the area v^* . For details see main text.

To account for drift – a necessary ingredient in adapting iHMMs to single molecule data analysis – the emission distributions of Eq. (3) must be coupled to a continuous process that acts like a “control” or “drive”. For simplicity, we call this the “control process”.

Below, we present the extensions needed to generalize the iHMM into ICON. Initially, we assume single trace observations (as would be the case if we were to look at a force spectroscopy time trace or a single channel from an smFRET experiment) and describe how we account for drift. Subsequently, we extend the treatment to more than one trace (as would be expected in dealing with donor and acceptor channels in smFRET). The method may be straightforwardly extended to the general case of more than two traces arising, for instance, with some single molecule fluorescent tweezers experiments [2, 24, 25] and experiments involving multiple FRET probes [26].

2.1 Single time trace

We first consider a single experimental trace with measurements $\bar{z} = (z_1, z_2, \dots, z_N)$. At each time step, the measurements $z_n = x_n + y_n$ consist of the biomolecular emissions x_n and drift y_n . Unlike emissions, which may abruptly change from time step to time step, the drift contribution to the time series, $\bar{y} = (y_1, y_2, \dots, y_N)$, evolves slowly. That is, drift evolves at a rate that is much slower than data acquisition. Assuming that the time scales at which the biomolecule and drift evolve are well separated, we may model each $y_n = f(t_n)$ as a point from a continuous function $f(t)$. Further, we may use the data to infer the shape of $f(t)$ within the Bayesian paradigm. The power of the method we propose here relies on two features: i) its generality which makes no assumptions about $f(t)$ besides continuity; and ii) the simultaneous learning of $f(t)$ (see below) with the rest of the model parameters as opposed to de-trending in pre-processing.

Although we intend to learn an arbitrary function $f(t)$, for computational reasons we use a finite approximation that is provided by interpolation. Given that interpolation provides approximations to any continuous function up to arbitrary degree [27], this choice offers a flexible means of performing inference on the drift that is amenable to computation.

More precisely, to model the drift function $f(t)$, we apply a set of nodes (t_m^*, y_m^*) , $m = 1, \dots, M$, and use cubic spline interpolation to approximate it across nodes, see Fig. 3. For sufficiently large M , the resulting $f(t)$ are practically indistinguishable [27]. Therefore the precise choice of M is of little or no importance with respect

to biophysical applications. Concerning the placement of the nodes, we note that t_m^* generally need not coincide with t_n . We also note that neither the interpolation needs to use splines as we will focus on here, but more general schemes can also be incorporated. For simplicity, in this study we assume that, once M is chosen, t_m^* are kept fixed and equidistantly placed over the time series. In contrast, the node heights y_m^* are treated as parameters with values that are to be inferred from the data.

In particular, to infer the values of y_m^* which ultimately determine the overall shape of $f(t)$, we place a normal prior

$$y_m^* | h^*, w^* \sim \mathcal{N}(h^*, w^*). \quad (7)$$

Here, h^* denotes the mean of the drift nodes and w^* the precision. That is, h^* influences the height at which nodes are placed and w^* how tightly the nodes are placed around this average. To infer both h^* and w^* , we specify a vague normal-gamma hyperprior.

The emission and drift models, resulting from Eqns. (3) and (7), without further specifications are ill-posed. Given that contributions to the total emission from \bar{x} and \bar{y} are assessed only through the observations $\bar{z} = \bar{x} + \bar{y}$, the whole model is invariant with respect to a translation of \bar{x} and \bar{y} equal in magnitude but opposite in direction. More precisely, the model gives identical outcomes for $\bar{x} + c$ and $\bar{y} - c$, for any arbitrary constant c . To resolve this issue, we may tether \bar{y} . That is, we may restrict the interpolation nodes y_m^* such that the area between the predicted \bar{y} and a reference level y_{ref}^* , which is given by $v^* = \sum_{n=1}^N (y_n - y_{\text{ref}}^*)(t_n - t_{n-1})$, is zero. Thus, in our formulation, the interpolation nodes y_m^* would not only satisfy the normal prior of Eq. (7) but also satisfy the condition $v^* | y_m^* = 0$. Finally, by setting $y_{\text{ref}}^* = 0$, we ensure that the drift trace remains near the zero emission level or equivalently we ensure that the estimated emission trace \bar{x} remains close – in fact, the closest possible – to the observation trace \bar{z} .

In summary, the drift model we describe above assumes that: i) the drift stems from a continuous process; ii) its shape is dictated by the data; and iii) it remains close to the level of zero emissions. Under those assumptions, we can readily model any type of drift such as monotonic or oscillatory drift, such as in Figs. 5 and 7 that follow, as the precise locations of y_m^* adapt to the supplied data.

The full set of equations describing ICON, including the equations of iHMM and the drift representation, is summarized in the supporting materials.

2.2 Multiple time traces

To handle observations collected by the same biomolecule contained in more than one parallel traces, we must extend the methodology presented above. Specifically, while the state transitions are coupled to all traces, we cannot assume that emission or drift models are coupled and must therefore learn these independently. Here we describe the necessary modifications.

For simplicity, we assume that only two traces $\bar{z}^1 = (z_1^1, z_2^1, \dots, z_N^1)$ and $\bar{z}^2 = (z_1^2, z_2^2, \dots, z_N^2)$ are available. The general case of more than two traces is a straightforward extension.

As with the case of the single trace, observations are decomposed into emissions and drift $\bar{z}^1 = \bar{x}^1 + \bar{y}^1$ and $\bar{z}^2 = \bar{x}^2 + \bar{y}^2$. To model each emission trace, we assume distributions $F_{\sigma_k}^1(x^1)$ and $F_{\sigma_k}^2(x^2)$ different for each

trace

$$x_n^1 | s_n \sim F_{s_n}^1, \tag{8}$$

$$x_n^2 | s_n \sim F_{s_n}^2, \tag{9}$$

where s_n denotes the conformation of the biomolecule at time t_n which is modeled as in the single trace case. To obtain, $F_{\sigma_k}^1(x^1)$ and $F_{\sigma_k}^2(x^2)$, we use the same generic family, Eq. (1); however, we apply different state specific parameters $\phi_{\sigma_k}^1$ and $\phi_{\sigma_k}^2$ on them. Furthermore, we use different prior distributions $H^1(\phi_\sigma^1)$ and $H^2(\phi_\sigma^2)$ for the parameters associated with each trace.

Similar to the case of the single trace, we model drift \bar{y}^1 and \bar{y}^2 using interpolation, but we place different sets of nodes (t_m^1, y_m^{*1}) and (t_m^2, y_m^{*2}) on them with unique priors for each

$$y_m^{*1} | h^{*1}, w^{*1} \sim \mathcal{N}(h^{*1}, w^{*1}), \tag{10}$$

$$y_m^{*2} | h^{*2}, w^{*2} \sim \mathcal{N}(h^{*2}, w^{*2}), \tag{11}$$

in addition to unique hyper-priors over h^{*1}, w^{*1} and h^{*2}, w^{*2} . Finally, to deal with drift tethering, we restrict each drift trace to remain close to the zero emission levels individually $v^{*1} | y_m^{*1} = 0$ and $v^{*2} | y_m^{*2} = 0$. The full set of equations describing ICON for double trace analysis is summarized in the supporting materials.

2.3 Computational considerations

For the analyses shown in the Results below, we implemented ICON described above using a Gibbs sampling scheme [28]. Specifically, to deal with the infinite dimensional state space $\{\sigma_1, \sigma_2, \dots\}$ we used the beam sampling algorithm [29] as described in our companion article [19] that provides step-by-step implementation details for these methods. Briefly, the beam sampling algorithm uses slicer variables to truncate $\{\sigma_1, \sigma_2, \dots\}$ to a finite size that is adjusted during the sampling iterations [21, 30]. To account for drift, we combined a Metropolis random walk step within the overall Gibbs scheme [28].

More details are provided in our companion perspectives article [19] and a working implementation of ICON, written in MATLAB[®], is provided in the supporting materials.¹

The methodology developed here offers flexibility in the modeling and analysis of single molecule data. Nevertheless, this flexibility comes with added computational cost, a disadvantage inherited from Gibbs sampling [28]. In particular, our algorithm spends most of its time updating the state sequence (s_1, s_2, \dots, s_N) . As explained in Ref. [29], this is performed by the forward filtering-backward sampling algorithm [31] which has a complexity of $O(NK^2)$. That is, the most costly part of our implementation scales linearly with the length of the trace N and quadratically with the number of states K that are needed to explain the observations. Despite this rather high complexity, a typical time trace from smFRET with 500–1000 data points, such as those analyzed below, take a reasonable time on an average desktop computer, ≈ 1 min, to sufficiently sample the posterior distribution.

We note that those components that make ICON differ from the simpler iHMM only trivially add to the computational burden. Rather, the bulk of the burden originates from the computational schemes required to characterize the posterior (i.e. sampling) of the iHMM itself. Computational Statistics is an active area of research with variational methods [32, 33] or approximate sampling schemes [34] actively considered as alternatives to brute

¹This code can also be found on the authors' website as well as on GitHub.

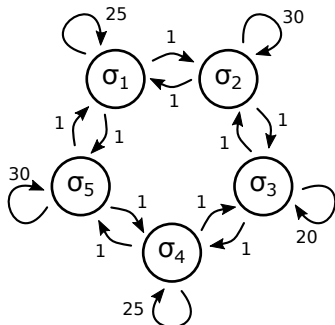


Figure 4: **Five-state Markov model generating the synthetic data that are used to benchmark ICON. The model transitions between five states σ_1 – σ_5 with transition probabilities proportional to the weights shown. For simplicity, only the state transitions shown (arrows) are allowed. The generated trace, after the addition of noise and drift, is shown on Fig. 5.**

force Gibbs sampling. On this basis, we believe that this burden of the iHMM will be substantially reduced in the near future.

3 Results

Below we present selected applications of the method whose mathematics are detailed in the previous section. Initially, to benchmark our method, we apply it to the analysis of synthetic data. We subsequently tackle experimental smFRET traces provided by the Nils Walter lab available online (see the supporting materials of Ref. [35]). These traces had previously been analyzed by traditional HMMs [35].

3.1 Synthetic data

We use state transitions of the Markov model shown on Fig. 4 to generate the signal underlying the synthetic trace. As for the noise, we assumed Gaussian emissions of different mean values and precisions associated with each state. In addition to noise, we contaminated the resulting trace with drift containing a linear trend as well as oscillations. The resulting trace is shown on Fig. 5 (upper panel). We choose five states with a reasonably high noise level, as can be seen in Fig. 5, specifically because fixing the number of states or subtracting drift *a priori* for the HMM would be difficult.

The middle panel of Fig. 5 shows the estimated most likely state sequence and drift. A comparison with the true emission trace (the trace plotting the means of the emissions of the states visited) reveals good agreement with only few occasional missed transitions. The lower panel shows how state estimation badly deteriorates had we ignored the drift altogether.

Unlike the HMM, the iHMM – from which ICON is derived — builds a full posterior distribution over the number of states present in the trace as shown in Fig. 6. In particular, in Fig. 6 (upper left panel), we show a histogram of the number of states estimated by ICON. As can be seen, ICON’s marginal posterior over the number of states is peaked at the correct number, 5. Since the iHMM models a state space of size that is not fixed, this number may take different values. For example, ICON provides low probabilities to other choices, 6, 7, 8, and 9, indicating that it is less likely the supplied data would have been generated by a system with this many states. Cases with fewer than 5 or more than 9 states effectively have no probability. Furthermore, by ignoring drift, the

corresponding estimates of Fig. 6 (upper right panel) shift toward higher numbers suggesting the recruitment of “artifact states”.

In addition, Fig. 6 (lower left panel) shows how the mean signal levels of each state are distributed. This figure clearly illustrates the locations of the state emissions which – consistent with the upper panel – identify 5 prominent peaks. As can be seen, ICON successfully identifies and localizes the emission distributions despite the large number of states and the presence of drift in the raw trace, Fig. 5 (upper panel).

The right panels of Fig. 6 illustrate just how inaccurate the inference becomes if we ignore drift. Here a plain iHMM with no drift correction clearly overestimates the number of states and misidentifies the emission distributions in large part by over-interpreting the location of the mean levels.

3.2 Experimental data

In the analysis of real data, we focused on smFRET measurements. In typical smFRET experiments, two parallel traces are available describing the same system: the donor and acceptor trace [5]. We denote the trace intensity levels recorded in the acceptor and donor channels as \bar{x}^1 and \bar{x}^2 , respectively. Both traces are commonly combined into a single “FRET efficiency” trace $\bar{x} = \bar{x}^1 / (\bar{x}^1 + \bar{x}^2)$.

For this study, we used selected experimental traces available from Ref. [35] which describes details of the sample preparation and data acquisition. We analyzed these traces with ICON utilizing either a single trace, for which we used the efficiency \bar{x} , or both acceptor \bar{x}^1 and donor \bar{x}^2 recordings. The same traces have been previously analyzed using traditional HMM with the results of the analysis available in Ref. [35].

3.2.1 FRET: single trace

Figure 7 (upper panel) displays individual acceptor and donor intensity recordings. Figures 7 (lower panel) and 8 show the resulting estimates provided by ICON. To obtain the estimates in these figures, we used ICON once assuming drift and once ignoring drift similar to the synthetic dataset of the previous section.

As can be seen, ICON with drift identifies 3 states located approximately at efficiencies 0.2, 0.4, and 0.7. As with the synthetic traces, ignoring the drift, the iHMM over-interprets the data and identifies 4 states instead located approximately at 0, 0.35, 0.65, and 0.9. The latter estimates are similar to the estimates provided in Ref. [35] obtained by means of traditional HMMs, which i) ignore drift and ii) fix the total number of states *a priori*.

A few points are in order here on the problems caused by drift for even the simple traditional HMM. First, drift in a time trace necessarily results in a closer fit of the model to the data when an initial larger number of states are introduced. Thus, without appropriately accounting for drift, a different number of states used to model the data across data sets may simply reflect the level of drift. Furthermore, regardless of the numbers of states used in an HMM analysis (even if a reasonable number of states are fixed *a priori*), the values for the FRET efficiencies – that ultimately are interpreted as inter-molecular distances – are off in the absence of drift correction.

3.2.2 FRET: multiple traces

Figure 9 (upper two panels) shows an example of acceptor and donor traces where the acceptor trace drifts heavily upward toward its beginning. We applied ICON on these traces, but instead of using the resulting FRET efficiency we utilized the recordings individually. As demonstrated in Fig. 9 (lower panel), our method identifies 3 states

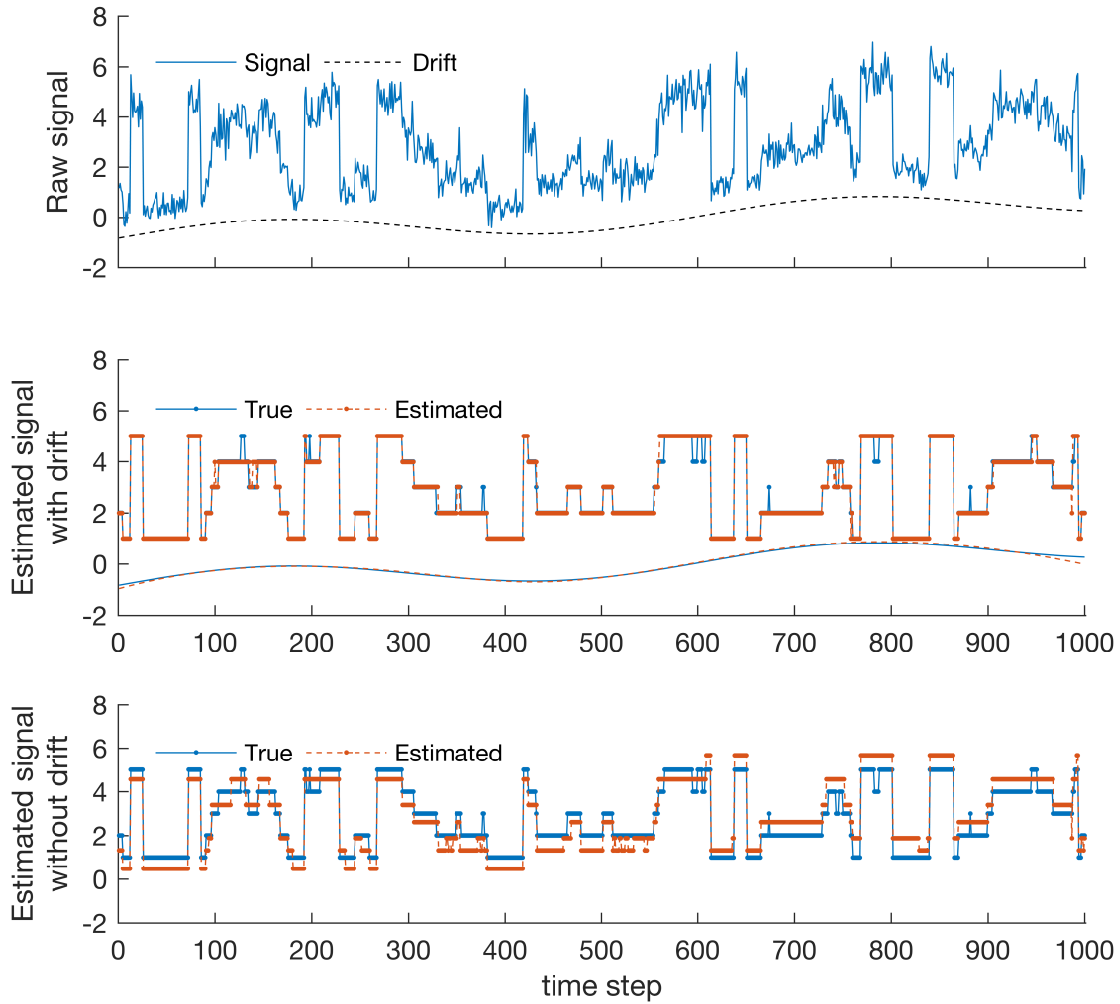


Figure 5: **ICON can analyze time traces contaminated with both noise and drift and self-consistently learn the drift while learning the number of states in addition to all other quantities determined by the HMM.** *Upper panel:* Synthetic time traces with drift were generated as described in Fig. 4. *Middle panel:* True (solid) and estimated (dashed) traces for the state sequence means and drift. *Lower panel:* Corresponding true and estimated trace for the state sequence means without drift estimation. Note that without drift correction, the iHMM over-interprets drift as the population of additional states. This over-interpretation is further quantified in Fig. 6 (left panels).

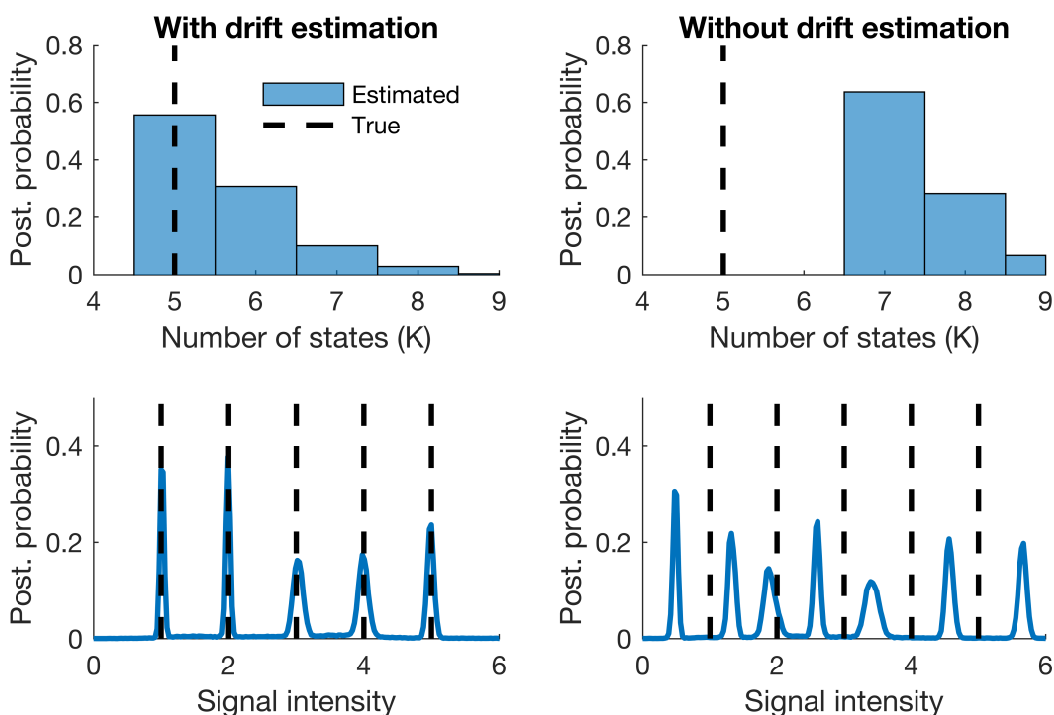


Figure 6: **ICON yields a full posterior distribution over states and their associated parameters.** *Upper panels:* Estimated number of states that generate the data in Fig. 5. *Lower panels:* Estimated locations of the emission mean levels. Both sets of results are shown for the ICON with drift estimation (left panels) and without (right panels). In all panels, dashed lines indicate the true values. The introduction of artifact states on the right panels is apparent which indicates the limits of the iHMM (i.e. ignoring drift) in the analysis of time series.

located at efficiencies of approximately 0.65, 0.75, and 0.80 as compared to the estimate of 0.55 and 0.75 (not shown) using a finite HMM where two states had previously been *a priori* imposed [35]. The difference in the efficiencies here is primarily ascribed to the drift that we corrected for in our method.

Again, to demonstrate the effects of ignoring drift, we analyzed the same traces disabling drift correction. In this case, the estimated number of states remains 3 and their locations are at 0.60, 0.65 and 0.75. Nevertheless, despite the apparent similarities, there is dramatic difference in the kinetics. For example, the lower panel compares the most likely signal sequence of the two cases. Due to the heavily drifted acceptor trace, essentially the whole trace is estimated to consist of two excessively long dwells and only a short transition to a third state.

Previously we had seen how drift may force the iHMM to populate artifact states. But in fact, drift can also do the opposite. As can be seen, with ICON, the biomolecule in Fig. 9 is estimated to alternate quickly between states for all times suggesting fast kinetics and shorter dwell times. By contrast, by ignoring drift the biomolecule is estimated to dwell in a single state throughout the entire first half of the trace, suggesting slow kinetics and a long dwell time for this state. In other words, the heavily drifting acceptor trace essentially homogenizes the data and makes transitions between states more difficult to detect.

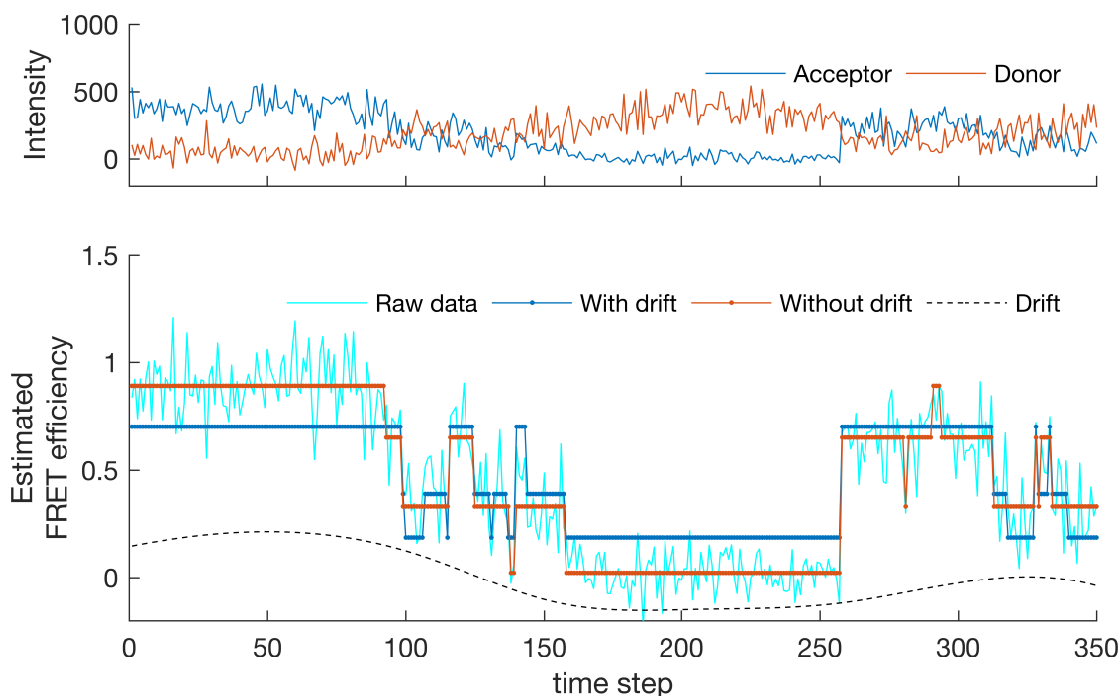


Figure 7: **ICON applied in the analysis of experimental smFRET time traces.** *Upper panel:* Raw acceptor and donor traces from smFRET measurements [35]. For the analysis, these traces were combined into a single FRET efficiency trace. *Lower panel:* Corresponding raw and estimated FRET efficiency. Here we show the results that consider drift (blue and black lines) and results that ignore drift (red line). Note how ignoring drift leads to over-interpretation of the higher and lower efficiency levels. This over-interpretation is further quantified in Fig. 8.

4 Discussion

The HMM has been a workhorse of time series analysis in single molecule Biophysics. Having started with the analysis of time series derived from single ion-channel patch clamp experiments [36, 37, 38], HMMs have then been used in the analysis of smFRET [5] and single molecule force spectroscopy [39], amongst other methods [40]. The HMMs greatest shortcoming – one that has been elegantly resolved by the iHMM [12] – is that the number of states attained need to be prespecified *a priori*. The challenge remains that, as is, the power of the iHMM cannot be directly harnessed to tackle single molecule problems.

The method presented here, ICON, generalizes the iHMM to deal with single molecule time traces directly by coupling the iHMM to a slow-evolving control process that accounts for drift. We also described how one may apply ICON to problems where multiple traces are provided on a single system like in smFRET.

Throughout this study we dealt with cases of drift evolving on a time scale slower than typical biomolecular dynamics, for example as in Fig. 5. However, this is not a limitation of the method. In fact, while less biophysically relevant perhaps, the method can also be applied with modifications to handle non-smooth drift or even drift that changes at time scales as fast as the dynamics themselves. This can be achieved by increasing the number of nodes in the interpolation, see Fig. 3, or by using a different set of basis functions in the interpolation of $f(t)$.

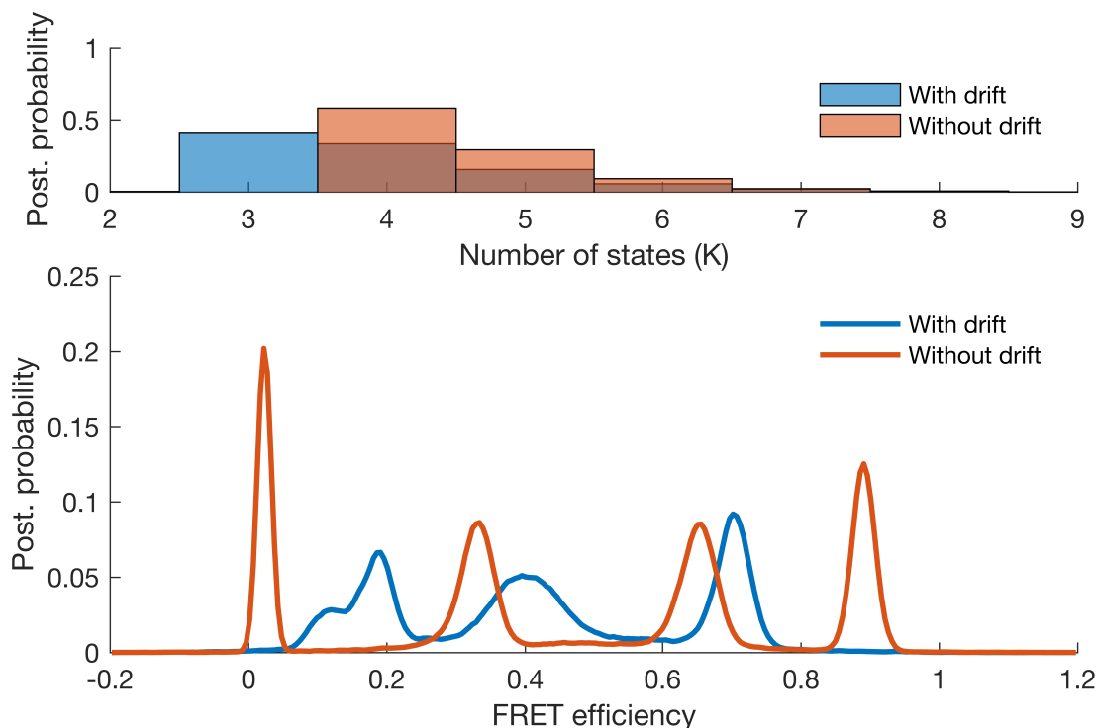


Figure 8: **Results of the ICON analysis on the experimental smFRET data of Fig. 7.** *Upper panel:* Estimated number of states. *Lower panel:* Estimated locations of the emission distributions. In both panels we show results incorporating drift (blue) and ignoring drift (red). Over-interpretation of the data in the latter case is apparent.

For example, cubic polynomials that are used in the analyses shown, can be replaced by Hermite polynomials or step functions and future work on these underdetermined problems will be dictated by their experimental need.

A few other methods outside Biophysics have considered continuous processes coupled to iHMMs as in the present study. These include the switching linear dynamical system (SLDS) [41] and its variants [42] which couple the dynamics of an array of linear systems with those of an iHMM. Specifically, SLDS uses linear dynamics to model traces of observations that evolve in a continuous manner which is best suited to describe mechanical systems. The formulation we adopted here was inspired by these methods but moves in a different direction as our goal is not to provide an accurate description of a system with well known dynamics but rather to provide a general modeling approach that relies on minimal assumptions about the time evolution of the drift. A more general method with less restrictive requirements is indeed demanded by single molecule experiments as assumptions on the drift's dynamics are difficult to make *a priori* [1, 18].

As we show in the previous section, ignoring drift can lead to dramatic differences in the outcome of the analysis. Most notably, in all cases examined – synthetic or real – drift forces the iHMM to introduce artifact states that give rise to erroneous kinetics or transitions between real and artifact states. With heavily drifting time series, these effects are exaggerated.

Drift correction in ICON fundamentally avoids the cherry-picking of raw time traces or pre-processing of traces that would otherwise occur when presented with traces that drift to varying degrees. To date, heavily drifted time series are either discarded from the analysis based on subjective criteria or corrected for drift in ad hoc and often

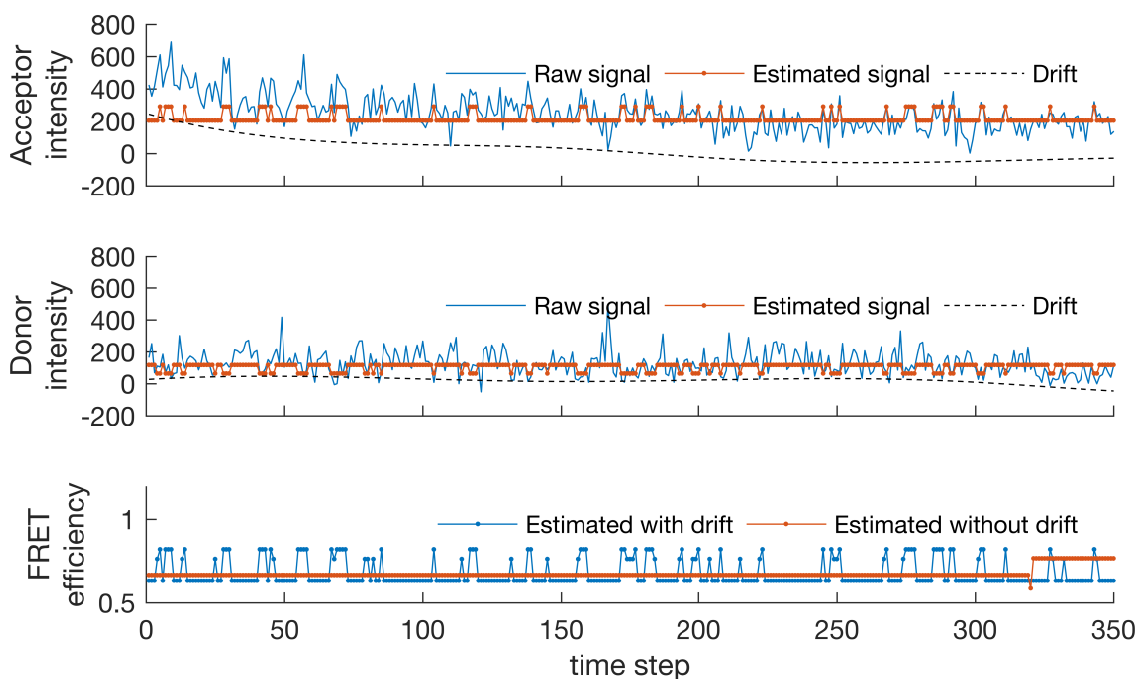


Figure 9: **Example of smFRET donor and acceptor traces analyzed individually by ICON.** *Upper panel:* Acceptor raw recordings and estimated signal. *Middle panel:* Donor raw recordings and estimated signal. *Lower panels:* Corresponding estimated FRET efficiency with drift and without drift estimation. Note the homogenization of the signal induced by the drifted acceptor trace in the latter case.

undocumented manner. Indeed, as we have demonstrated, the analysis of traces with drift under the appropriate correction leads to accurate results and thus there is no need to discard traces on an arbitrary basis. What is more, state determination in ICON also avoids post-processing model selection steps to determine the number of states using tools such as maximum evidence as for example in Ref. [4].

Finally, to account for multiple experimental traces, we coupled the emissions to several observation traces to specifically deal with data such as smFRET. In doing so, we fitted separate emission distributions and drift in each trace individually. The method presented here is general in that it assumes no correlation in the different traces. However, in many application there might be additional structure shared between observations besides what we have represented in the present study. For example, in FRET measurements, donor and acceptor emissions are strongly anti-correlated [1]. In such cases, incorporating further assumptions on the model, for example by explicitly forcing the model to fit anti-correlated emission distributions, could lead to improved inference. Such modifications are readily accommodated within ICON.

It took roughly thirty years for the theoretical breakthrough – that is Bayesian nonparametrics [11] and the Dirichlet process [14] – to become computationally tractable and have a deep impact in data science. With powerful computational tools at hand and many more active researchers in the field, it is our expectation that it will take a fraction of that time for nonparametrics to make an equally important contribution to single molecule Biophysics.

References

- [1] R Roy, S Hohng, and T Ha. A practical guide to single-molecule FRET. *Nature Methods*, 5(6):507–516, 2008.
- [2] KC Neuman and A Nagy. Single-molecule force spectroscopy: optical tweezers, magnetic tweezers and atomic force microscopy. *Nature Methods*, 5(6):491, 2008.
- [3] L Rabiner and B Juang. An introduction to hidden Markov models. *IEEE ASSP Magazine*, 3(1):4–16, 1986.
- [4] JE Bronson, J Fei, JM Hofman, RL Gonzalez, and CH Wiggins. Learning rates and states from biophysical time series: a Bayesian approach to model selection and single-molecule fret data. *Biophysical Journal*, 97(12):3196–3205, 2009.
- [5] M Blanco and NG Walter. Analysis of complex single-molecule FRET time trajectories. *Methods in Enzymology*, 472:153–178, 2010.
- [6] JW Yoon, A Bruckbauer, WJ Fitzgerald, and D Klenerman. Bayesian inference for improved single molecule fluorescence tracking. *Biophysical Journal*, 94(12):4932–4947, 2008.
- [7] RA Rosales. MCMC for hidden Markov models incorporating aggregation of states and filtering. *Bulletin of Mathematical Biology*, 66(5):1173–1199, 2004.
- [8] KE Hines. A primer on Bayesian inference for biophysical systems. *Biophysical Journal*, 108(9):2103–2113, 2015.
- [9] SA McKinney, C Joo, and T Ha. Analysis of single-molecule FRET trajectories using hidden Markov modeling. *Biophysical Journal*, 91(5):1941–1951, 2006.
- [10] JB Munro, RB Altman, N O'Connor, and SC Blanchard. Identification of two distinct hybrid state intermediates on the ribosome. *Molecular Cell*, 25(4):505–517, 2007.
- [11] TS Ferguson. Bayesian density estimation by mixtures of normal distributions. *Recent Advances in Statistics*, 24(1983):287–302, 1983.
- [12] MJ Beal, Z Ghahramani, and CE Rasmussen. The infinite hidden Markov model. In *Advances in Neural Information Processing Systems*, pages 577–584, 2001.
- [13] KE Hines, JR Bankston, and RW Aldrich. Analyzing single-molecule time series via nonparametric Bayesian inference. *Biophysical Journal*, 108(3):540–556, 2015.
- [14] YW Teh, MI Jordan, MJ Beal, and DM Blei. Hierarchical Dirichlet processes. *Journal of the American Statistical Association*, 2012.
- [15] Randal Douc, Eric Moulines, and David Stoffer. *Nonlinear time series: theory, methods and applications with R examples*. CRC Press, 2014.
- [16] Zhaohua Wu, Norden E Huang, Steven R Long, and Chung-Kang Peng. On the trend, detrending, and variability of nonlinear and nonstationary time series. *Proceedings of the National Academy of Sciences*, 104(38):14889–14894, 2007.
- [17] JD Hamilton. *Time series analysis*, volume 2. Princeton University Press Princeton, 1994.
- [18] SJ Holden, S Uphoff, J Hohlbein, D Yadin, L Le Reste, OJ Britton, and AN Kapanidis. Defining the limits of single-molecule FRET resolution in TIRF microscopy. *Biophysical Journal*, 99(9):3102–3111, 2010.
- [19] I Sgouralis and S Pressé. An introduction to iHMMs for single molecule data analysis. *Biophysical Journal* (Submitted), 2016.

- [20] M Sen, RA Maillard, K Nyquist, P Rodriguez-Aliaga, S Presse, A Martin, and C Bustamante. The ClpXP protease unfolds substrates using a constant rate of pulling but different gears. *Cell*, 155(3):636–646, 2013.
- [21] RM Neal. Markov chain sampling methods for Dirichlet process mixture models. *Journal of Computational and Graphical Statistics*, 9(2):249–265, 2000.
- [22] PA Chong and JD Forman-Kay. A new phase in ALS research. *Structure*, 24(9):1435–1436, 2016.
- [23] D Görür and CE Rasmussen. Dirichlet process gaussian mixture models: Choice of the base distribution. *Journal of Computer Science and Technology*, 25(4):653–664, 2010.
- [24] MSZ Kellermayer, SB Smith, HL Granzier, and C Bustamante. Folding-unfolding transitions in single titin molecules characterized with laser tweezers. *Science*, 276(5315):1112–1116, 1997.
- [25] MJ Comstock, KD Whitley, H Jia, J Sokoloski, TM Lohman, T Ha, and YR Chemla. Direct observation of structure-function relationship in a nucleic acid-processing enzyme. *Science*, 348(6232):352–354, 2015.
- [26] NK Lee, AN Kapanidis, HR Koh, Y Korlann, SO Ho, Y Kim, N Gassman, SK Kim, and S Weiss. Three-color alternating-laser excitation of single molecules: monitoring multiple interactions and distances. *Biophysical Journal*, 92(1):303–312, 2007.
- [27] Kendall Atkinson and Weimin Han. *Theoretical numerical analysis*, volume 39. Springer, 2005.
- [28] Ch Robert and G Casella. *Monte Carlo statistical methods*. Springer Science & Business Media, 2013.
- [29] J Van Gael, Y Saatchi, YW Teh, and Z Ghahramani. Beam sampling for the infinite hidden Markov model. In *Proceedings of the 25th International Conference on Machine Learning*, pages 1088–1095. ACM, 2008.
- [30] SG Walker. Sampling the Dirichlet mixture model with slices. *Communications in Statistics–Simulation and Computation*, 36(1):45–54, 2007.
- [31] CK Carter and R Kohn. On Gibbs sampling for state space models. *Biometrika*, 81(3):541–553, 1994.
- [32] N Ding and Z Ou. Variational nonparametric Bayesian hidden Markov model. In *2010 IEEE International Conference on Acoustics, Speech and Signal Processing*, pages 2098–2101. IEEE, 2010.
- [33] M Johnson and AS Willsky. Stochastic variational inference for Bayesian time series models. In *ICML*, pages 1854–1862, 2014.
- [34] N Tripuraneni, S Gu, H Ge, and Z Ghahramani. Particle gibbs for infinite hidden markov models. In *Advances in Neural Information Processing Systems*, pages 2395–2403, 2015.
- [35] MR Blanco, JS Martin, ML Kahlscheuer, R Krishnan, J Abelson, A Laederach, and NG Walter. Single molecule cluster analysis dissects splicing pathway conformational dynamics. *Nature Methods*, 2015.
- [36] F Qin, A Auerbach, and F Sachs. A direct optimization approach to hidden Markov modeling for single channel kinetics. *Biophysical Journal*, 79(4):1915–1927, 2000.
- [37] L Venkataramanan and FJ Sigworth. Applying hidden Markov models to the analysis of single ion channel activity. *Biophysical Journal*, 82(4):1930–1942, 2002.
- [38] Shin-Ho Chung, John B Moore, Lige Xia, LS Premkumar, and PW Gage. Characterization of single channel currents using digital signal processing techniques based on hidden Markov models. *Philosophical Transactions of the Royal Society of London B: Biological Sciences*, 329(1254):265–285, 1990.
- [39] M Kruithof and J van Noort. Hidden Markov analysis of nucleosome unwrapping under force. *Biophysical Journal*, 96(9):3708–3715, 2009.

- [40] M Tavakoli, JN Taylor, CB Li, T Komatsuzaki, and S Pressé. Single molecule data analysis: An introduction. *arXiv preprint arXiv:1606.00403*, 2016.
- [41] E Fox, EB Sudderth, MI Jordan, and AS Willsky. Nonparametric Bayesian learning of switching linear dynamical systems. In *Advances in Neural Information Processing Systems*, pages 457–464, 2009.
- [42] E Fox, EB Sudderth, MI Jordan, and AS Willsky. Bayesian nonparametric inference of switching dynamic linear models. *IEEE Transactions on Signal Processing*, 59(4):1569–1585, 2011.